Received: 18 April 2022 | Revised: 22 August 2022 | Accepted: 28 August 2022

DOI: 10.1002/pro.4438

FULL-LENGTH PAPER

THE PROTEIN SOCIETY WILEY

Ostrinia furnacalis PBP2 solution NMR structure: Insight into ligand binding and release mechanisms

Salik R. Dahal | Jacob L. Lewellen | Shine Ayyappan | Bharat P. Chaudhary | Viswanath Nukala | Smita Mohanty

Department of Chemistry, Oklahoma State University, Stillwater, Oklahoma, USA

Correspondence
Smita Mohanty, Department of Chemistry, Oklahoma State University, Stillwater, OK 74078, USA.
Email: smita.mohanty@okstate.edu

Funding information
National Science Foundation, Grant/Award Numbers: CHE-1807722, DBI-1726397; National Science Foundation Cooperative, Grant/Award Number: DMR-1644779

Review Editor: Carol Post

Abstract

Ostrinia furnacalis is an invasive lepidopteran agricultural pest that relies on olfaction for mating and reproduction. Male moths have an extremely sensitive olfactory system that can detect the sex pheromones emitted by females over a great distance. Pheromone-binding proteins present in the male moth antenna play a key role in the pheromone uptake, transport, and release at the dendritic membrane of the olfactory neuron. Here, we report the first high-resolution NMR structure of a pheromone-binding protein from an *Ostrinia* species at pH 6.5. The core of the *Ostrinia furnacalis* PBP2 (OfurPBP2) consists of six helices, α1a (2–14), α1b (16–22), α2 (27–37), α3 (46–60), α4 (70–80), α5 (84–100), and α6 (107–124) surrounding a large hydrophobic pocket. The structure is stabilized by three disulfide bridges, 19–54, 50–108, and 97–117. In contrast to the unstructured C-terminus of other lepidopteran PBPs, the C-terminus of OfurPBP2 folds into an α-helix (α7) at pH 6.5. The protein has nanomolar affinity towards both pheromone isomers. Molecular docking of both pheromones, *E*-12 and *Z*-12-tetradecenyl acetate, to OfurPBP2 revealed that the residues Met5, Lys6, Met8, Thr9, Phe12, Phe36, Trp37, Phe76, Ser115, Phe118, Lys119, Ile122, His123, and Ala128 interact with both isomers, while Thr9 formed a hydrogen bond with the acetate head group. NMR structure and thermal unfolding studies with CD suggest that ligand release at pH 4.5 is likely due to the partial unfolding of the protein.

KEYWORDS
insect olfaction, NMR structure, NOE, *Ostrinia furnacalis*, pheromone-binding proteins (PBPs)

1 | INTRODUCTION

Olfaction provides a vital means of perception and communication in animals. Indeed, many animals employ this sensory system to locate food sources, avoid predators, identify mates, and promote reproduction. Lepidopteran moths rely on their olfactory system for the detection of minute quantities of sex pheromones over long distances. The sex pheromones secreted by the females initiate the mating process in moths.[1] Male antennae detect these pheromones with remarkable specificity.[2] Male antennae is covered with many sensory hairs and each sensory hair contains numerous pores. When the hydrophobic pheromones diffuse through

Salik R. Dahal and Jacob L. Lewellen equally contributed to this work.

these olfactory pores, pheromone-binding proteins (PBPs) present in high concentration in sensillar lymph of male moth antennae bind and transport them to the olfactory receptor neuron (ORN).[3]

Many lepidopterans are aggressive agricultural pests, costing billions of dollars annually.[4,5] The Asian corn borer (*Ostrinia furnacalis* Guenée) is a highly destructive polyphagous pest, widespread throughout Asia, Australia, and Oceania. *O. furnacalis* is difficult to control with broad-spectrum insecticides and is becoming resistant to common control measures.[6] Disrupting the mating process via inhibition of pheromone detection offers an alternative strategy for biorational control.

Lepidopteran PBPs are small acidic proteins composed of 130–150 amino acids with molecular weights of 13–20 kDa. These water-soluble proteins are composed of six or seven helices surrounding a hydrophobic binding pocket. Although these proteins have over 50% sequence identity and six strictly conserved cysteines that form disulfide bonds[7] (Figure 1), the chemical structure of their substrates are quite different. Of the five reported *O. furnacalis* PBPs (OfurPBPs), only OfurPBP2 and OfurPBP3 have male-biased expression and are involved in sex pheromone detection.[8,9] However, *O. furnacalis* is unique within *Ostrinia* since it has evolved to use a blend of *E*-12 and *Z*-12-tetradecenyl acetate (*E*-12- and *Z*-12-14: OAc) pheromones as opposed to *E*-11 and *Z*-11-tetradecenyl acetate (*E*-11- and *Z*-11-14: OAc) used by the remaining species of the genus.[8,10,11,12,13] This subtle change in the pheromone structure may correspond to distinct structural features in OfurPBP2. OfurPBP2 shares about 50% sequence identity to well-studied lepidopteran PBPs and retains six strictly conserved cysteine residues.[14,15,16] Despite high sequence similarity to other well-studied lepidopteran PBPs,[14,15,16] OfurPBP2 has remarkable differences in both biological gates (Figure 1).[8,17,14] Specifically, His70, which forms the histidine-gate with His95, is replaced by an arginine in OfurPBP2. Moreover, the C-terminal gate contains four additional charged residues, unlike other well-characterized lepidopteran PBPs[16,18,19] (Figure 1). These two gates have been reported to be critical for ligand-binding at higher pH and release at lower pH.[20,21] It has been shown for *Anthereae polyphemus* PBP1 (ApolPBP1), *Bombyx mori* PBP (BmorPBP), and *Amyelois transitella* PBP1 (AtraPBP1) that these proteins bind ligand at pH above 6.0 in PBP^B conformation (open or bound form) and release it at pH 4.5 while undergoing a pH-driven conformational switch to PBP^A (closed or free form).[20,21] In these proteins, the C-terminal gate is opened at pH above 6.0 with the unstructured C-terminus exposed to the solvent in the PBP^B conformation, allowing the ligand to enter the binding pocket. However, at acidic pH, the newly formed C-terminal helix occupies the

```
OfurPBP2        SQAVMKDMTKNFIKAYEVCAKEYNLPEAAGAEVMNFWKEGYVL-TSREAGCAILCLSSKL   59
ApolPBP1        SPEIMKNLSNNFGKAMDQCKDELSLPDSVVADLYNFWKDDYVM-TDRLAGCAINCLATKL   59
BmorPBP         SQEVMKNLSLNFGKALDECKKEMTLTDAINEDFYNFWKEGYEI-KNRETGCAIMCLSTKL   59
AtraPBP1        SPEIMKDLSINFGKALDTCKKELDLPDSINEDFYKFWKEDYEI-TNRLTGCAIKCLSEKL   59
BmorGOBP2       TAEVMSHVTAHFGKTLEECREESGLSVDILDEFKHFWSDDFDV-VHRELGCAIICMSNKF   59
LUSHOBP         --MTMEQFLTSLDMIRSGCAPKFKLKTE---DLDRLRVGDFNFPPSQDLMCYTKCVSLMA   59

OfurPBP2        NLLDPEGTLHRGNTVEFAKQHGSDDAMAHQLVDIVHACEKSVPPNEDNCLMALGISMCFK   119
ApolPBP1        DVVDPDGNLHHGNAKDFAMKHGADETMAQQLVDIIHGCEKSAPPNDDKCMKTIDVAMCFK   119
BmorPBP         NMLDPEGNLHHGNAMEFAKKHGADETMAQQLIDIVHGCEKSTPANDDKCIWTLGVATCFK   119
AtraPBP1        EMVDADGKLHHGNAREFAMKHGADDAMAKQLVDLIHGCEKSIPPNDDRCMEVLSIAMCFK   119
BmorGOBP2       SLMDDDVRMHHVNMDEYIKGFPNGQVLAEKMVKLIHNCEKQFDTETDDCTRVVKVAACFK   114
LUSHOBP         GTVNKKGEFNAPKALAQL-PHLVPPEMMEMSRKSVEACRDTHKQFKESCERVYQTAKCFS   114

OfurPBP2        TEIHKLNWAPDHELLLEEMMAEMKQ  144
ApolPBP1        KEIHKLNWVPNMDLVIGEVLAEV--  142
BmorPBP         AEIHKLNWAPSMDVAVGEILAEV--  142
AtraPBP1        KEIHNLKWAPNMEVVVGEVLAEV--  142
BmorGOBP2       KDSRKEGIAPEVAMIEAVIEKY---  141
LUSHOBP         ENADGQFMWP---------------  124
```

FIGURE 1 Primary sequences of the PBPs of the moths: *Ostrinia furnacalis* (Acc. Num. LC027679), *Antheraea polyphemus* (Acc. Num. X17559), *Bombyx mori* (Acc. Num. X94987), *Amyelois transitella* (Acc. Num. GQ433364), *Bombyx mori* GOBP2 (Acc. Num. X94989), and LUSH OBP (Acc. Num. AF001621), conserved cysteines are shown in red, histidine gate residues (His70 and His95) are highlighted in red background. The C-terminal gate is shown in the yellow background, with charged residues highlighted in red

pocket, causing the dissociation and release of the ligand through the opened histidine gate in the PBP^A conformation.[21] To understand the impact of histidine and C-terminal gate substitutions on OfurPBP2 structure and function, a detailed investigation was carried out. Here, we report the high-resolution structure and functional characterization of OfurPBP2 using circular dichroism (CD), fluorescence, nuclear magnetic resonance (NMR), and computational techniques. Surprisingly, the OfurPBP2 C-terminus at pH 6.5 forms a well-structured helix outside the hydrophobic pocket, in stark contrast to the unstructured C-terminus previously observed in lepidopteran PBPs.[16,18,22,23] Docking studies provided important insight into the similarities and differences in the binding interactions of the protein to both pheromone isomers.

2 | RESULTS

2.1 | Pheromone-binding affinity

Recombinant OfurPBP2 for the binding assay was expressed in bacteria and purified following the previously reported method.[14,17] Delipidation was carried out to remove the lipid bound to the protein from the bacterial cells.[21,24] The successful delipidation of OfurPBP2 was verified by 2D {^{1}H, ^{15}N} HSQC (Figure S1).

OfurPBP2 affinities to both E and Z pheromone isomers (E12–14: OAc and Z12–14: OAc) were determined by competitively displacing the N-phenyl-1-naphthylamine (NPN) fluorescent probe from the OfurPBP2:NPN complex at both pH 6.5 and 4.5 using fluorescence-based binding assays. At pH 6.5, the dissociation constants (K_d) obtained were 47.3 and 33.5 nM for E12–14: OAc and Z12–14: OAc, respectively (Figure 2). However, at pH 4.5, the dissociation constants could not be determined as the pheromones were unable to displace the NPN from the OfurPBP2:NPN complex (Figure S2).

2.2 | Thermal unfolding of OfurPBP2

To study the thermal unfolding of the OfurPBP2, the temperature dependence of the CD signal in the far UV region was used. Thermal unfolding of OfurPBP2 at pH 6.5 and 4.5 was monitored at 222 nm, as shown in Figure 3, Figures S3 and S4. The melting temperature (T_m) was found to be 87 and 90°C at pH 4.5 and pH 6.5, respectively. The thermodynamic parameters of unfolding were calculated from the data. The $\Delta G_{unfolding}$ of the protein at pH 6.5 and pH 4.5 were 47.1 ± 1.9 and 32.3 ± 0.8 kJ/mol, respectively.

2.3 | NMR structure determination

In OfurPBP2, 97% of backbone and 88% of side-chain resonances were assigned using various 3D NMR experiments as reported previously.[17] Analysis of the NOESY data showed strong sequential $d_{\alpha\delta}$ NOEs for all proline residues in OfurPBP2. The $^{13}C_\beta$ chemical shifts of all six cysteine were identified by NOE patterns. The characteristic downfield-shifted $^{13}C_\beta$ chemical shifts indicated that all cysteines are in the oxidized form.[25] The three-dimensional structure of OfurPBP2 was determined using NOEs, dihedral angles, and hydrogen bonds as restraints. The structure obtained has a resolution of 1.5 Å with root mean square deviations (rmsd) of 0.48 and 1.1 Å for backbone and heavy atoms, respectively. Table 1 summarizes

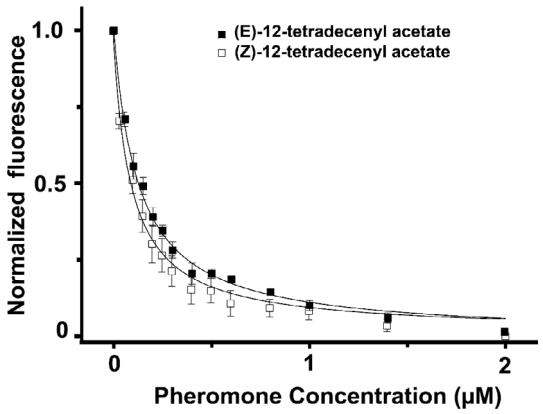

FIGURE 2 Competitive binding of pheromones (Z12-14: OAc and E12-14: OAc) with NPN. The error bar indicates the standard deviations. The emission spectra were collected in the range of 370–600 nm upon excitation at 337 nm. Quenching in the NPN fluorescence was monitored at 420 nm. The plot was fitted using non-linear fitting module of Origin 2019 as described under Section 4

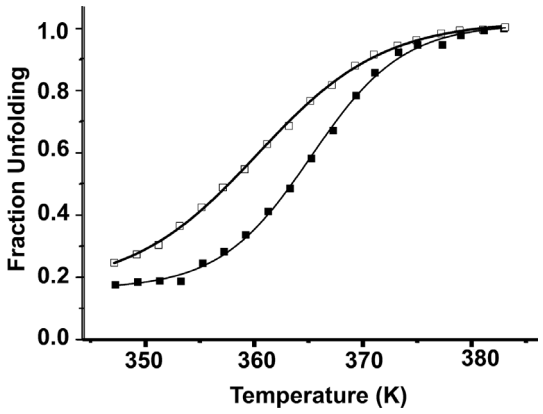

FIGURE 3 Plot of the fraction of unfolded protein as a function of temperature determined using the dichroic activity at 222 nm. (■) represent pH 6.5. (□) represent pH 4.5

TABLE 1 Restraints and structural statistics for OfurPBP2

Properties	Values
Restraints	
Total experimental distance restraints	2,557
Sequential $\|i-j\|<1$	1,314
Medium range $1<\|i-j\|<5$	841
Long range $\|i-j\|>5$	402
Dihedral angle restraints (Φ and Ψ)	260
Hydrogen bond distance restraints	80
Residual restraint violations after simulated annealing	
Distance restraint violation greater than 0.01 Å	6.0
Maximum distance restraint violation (Å)	0.33
Dihedral angle restraint violations	0.0
RMSD of backbone atoms from ideal geometry	
Bond length (Å)	0.009
Bond angles (°)	1.5°
RMS deviations from the averaged coordinates (Å)	
Backbone of the residues 1–130	0.48
All heavy atoms of the residues 1–130	1.10
Residual target function value ($Å^2$)	2.92
Total energy (kJ/mol)	−18,360.68
Ramachandran plot statistics (%)	
Most favored regions	97.7
Additionally allowed regions	2.3
Generously allowed regions	0.0
Disallowed regions	0.0

the structural statistics of the 20 lowest energy conformers. The three-dimensional structures of OfurPBP2 have been deposited in the RCSB Protein Data Bank (7UO6).

The strong and the medium-range NOE connectivity indicates the presence of seven helices, with the C-terminal helix, α7, formed by the polypeptide segment 131–143. Lack of long-range NOEs, from His131 to Gln144 implies a flexible C-terminus; however, several d_{NN} (i, $i+2$), $d_{\alpha N}$ (i, $i+2$), $d_{\alpha N}$ (i, $i+4$), and $d_{\alpha\beta}$ (i, $i+3$) NOEs in this region confirm an α-helical structure (Figure S5). Furthermore, the Lys38–Ser45 segment has few medium-range NOEs, and no long-range NOEs, which indicates an unstructured region.

2.4 | Overall structure of OfurPBP2 at pH 6.5

At pH 6.5, the OfurPBP2 core structure consists of six α-helices with residues 2–14 (α1a), 16–22(α1b), 27–37 (α2), 46–60 (α3), 70–80 (α4), 84–100 (α5), and 107–124 (α6). The C-terminus of the protein forms the seventh helix consisting of residues 131–143 (α7). The loops connecting the helices are named L1, L2, L3, and so on. L1 connects helices between α1and α2 and so on. All the seven helices of OfurPBP2 have C-capping hydrogen bond interactions. In addition, the α6 contains both C-capping and N-capping hydrogen bond interactions. These capping interactions play a central role in the stabilization of helices.

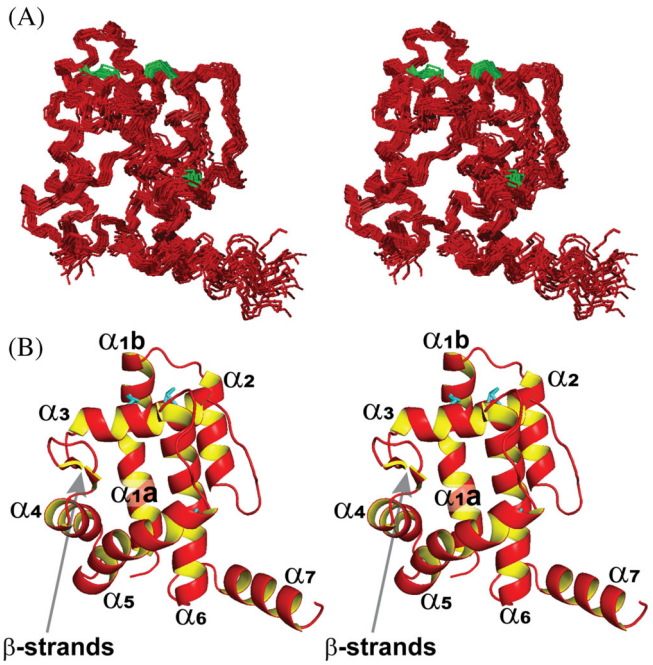

FIGURE 4 Stereo views of the three-dimensional structures of OfurPBP2. (A) Superposition of the 20 energy-minimized and water-refined conformations of OfurPBP2. Backbone residues are shown as red, and disulfide bonds are shown in green. (B) Ribbon drawing of one of the OfurPBP2 structures, where disulfide bonds are highlighted in cyan. The beta-flap is pointed by the arrow. The figure was prepared using Pymol

The protein is globular with approximate dimensions of (33 × 39 × 53) Å. Three disulfide bonds stabilize the helices and maintain the overall architecture of the protein. The six cysteine residues are conserved throughout the PBPs and form three disulfide bridges. The α1, α3, and α6 helices are anchored by two disulfide bonds between Cys19–Cys54 and Cys50–Cys108. Similarly, the third disulfide bond, Cys-97–Cys-117, connects α5 and α6, providing structural rigidity to the protein. A large hydrophobic cavity is formed by the six helices encompassing residues 1–130. Stereo views of the superposition of 20 lowest energy-minimized structures and a ribbon diagram of the overall structure are shown (Figure 4). The N-terminal segment (3–22) forms an amphipathic helix (Figure 4, Figure S6A) but has slight distortion in

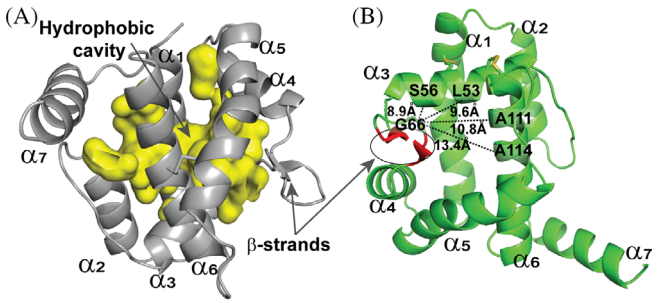

FIGURE 5 The three-dimensional structures of OfurPBP2. (A) Pheromone binding cavity of OfurPBP2; the surface of the hydrophobic cavity is shown in yellow. (B) The position of β-flap region of ofurPBP2 (shown in red) relative to the hydrophobic cavity

the middle (at Tyr16) similar to AtraPBP1[23] and BmorPBP.[26] The most interesting and prominent feature in the OfurPBP2 structure is its C-terminus (131–143) with well-defined sequential d_{NN} $(i, i + 1)$ NOEs (Figure S5) forms an amphipathic helix (Figure S6B). This C-terminal helix shows no long-range NOEs to the core of the protein, thus located outside the hydrophobic pocket exposed to the solvent (Figure 5).

The helices in the core of the protein are packed closely with the crossing angles of 34° between α1b–α2, 88°(α2–α3), 102°(α3–α4), 122°(α4–α5), and 126°(α5–α6). The α1 helix is slightly distorted at 27° (α1a-α1b), likely due to the Cys19–Cys54 disulfide bridge that pulls the α1b helix towards α3. Residues Thr73, Val74, and Ala77 of α4 and Ala87, Leu90, and Val91 of α5 pack in a knobs-into-holes manner, while residues Ile93, Val94, and Cys97 of α5 and Cys117, Phe118, and Glu121 of α6 are packed in ridges-into-grooves fashion (Figure S6C,D). These residues are well-conserved in lepidopteran PBPs, including BmorPBP.[26] Helices α1 and α3 pack at an angle of 95° through hydrophobic interactions between Tyr16, Cys19, Ala15 of α1 and Cys54, Ala51, and Leu55 of α3. There is also an electrostatic interaction between Glu22 (α1) and Lys58 (α3). The α2 and α3 helices pack at 88° and form a tiny hydrophobic core along with residues from α1. Residues involved in the formation of this core are Tyr16 and Cys19 from helix α1, Val33 from α2, and Ala48, Ala51, Ile52, and Leu55 from α3. Helices α3 and α6 cross at 85° with residues Gly49, Ile52, Leu53 of α3 having hydrophobic interactions with Cys108 and Ala111 of α6. The sidechain of Lys119 of α6 forms the cation–π interaction with the aromatic ring of the Phe36, the terminal residue of the α2, which provides additional stability to the core structure.

The primary sequence of OfurPBP2 contains 7 aspartates, 15 glutamates, 11 lysine, 2 arginine, and 6 histidine residues. Of these charged residues, three pairs are involved in the formation of the salt bridges: Glu22-Lys58, Arg46-Asp106, and Asp84-Lys78. The salt bridges, Glu22-Lys58 and Arg46-Asp106, are common for both OfurPBP2 and ApolPBP1.[16] Two amino acids, His123 and Lys119 are partially solvent accessible, while the remaining are found at the surface of the protein and are fully solvent-accessible, which accounts for the high solubility of the protein in water. The activities of many proteins are modulated by pH through the protonation and deprotonation of the histidine sidechain.[27] The histidine acts as a general acid–base by either donating or accepting a proton. There are two hydrogen bonds between Asp63-His69 and Asp92-His88 that keep the imidazole ring in a fixed orientation.

The hydrophobic cavity is lined with several aromatic residues including Phe12, Phe36, Trp37, Phe76, Phe118, and Trp127, which are highly conserved among lepidopteran PBPs. The aromatic ring of the Phe76 is orthogonal to Phe12. Moreover, Phe12 and Phe118 are sandwiched, forming a strong π–π interaction. These residues in the pocket are responsible for nonspecific binding. The Trp37 and Lys6 are solvent accessible and strictly conserved in Lepidopteran PBP; both of these residues form the opening of one end of the hydrophobic cavity.

Residues 61–69 (L3) connecting α3 and α4 form a β flap. L3 closely resembles a flap projecting over one of the openings of the hydrophobic pocket (Figure 6). This flap is flexible and allows for hinge-like motion, which may be responsible for the hydrophobic specificity. L3 has three distinct regions: residues 62–63 are in a β-strand conformation, residues 64–66 form a turn, and residues 67–68 are again in a β-strand conformation. The antiparallel β-strand conformation is stabilized by three hydrogen bonds: Gly66 H^N–Asp63 O, Asp63 O-Glu65 H^N, and Asp63 H^N–Thr67 O. Furthermore, the sidechain of Thr67 and the main chain NH of Asp63 interact to enforce this conformation. This antiparallel β-strand conformation in L3 encompassing residues 61–69 is reminiscent of BmorPBP complex.[25]

The flap residues together with His69, Arg70, His88, and His95 may play a major role in controlling the opening and closing of the pocket. These residues are conserved throughout the PBPs except Arg70, which is a His70 in many well-studied lepidopteran species.[14–16] Furthermore, these flap residues may play a role in ligand recognition and facilitate ligand entry or exit into or out of the pocket.

2.5 | The binding pocket of OfurPBP2

The OfurPBP2 has a large horseshoe-shaped hydrophobic cavity (Figure 5). The mouth of the cavity formed by the α3 helix, loop L3, and the N-terminus of α6 helix opens

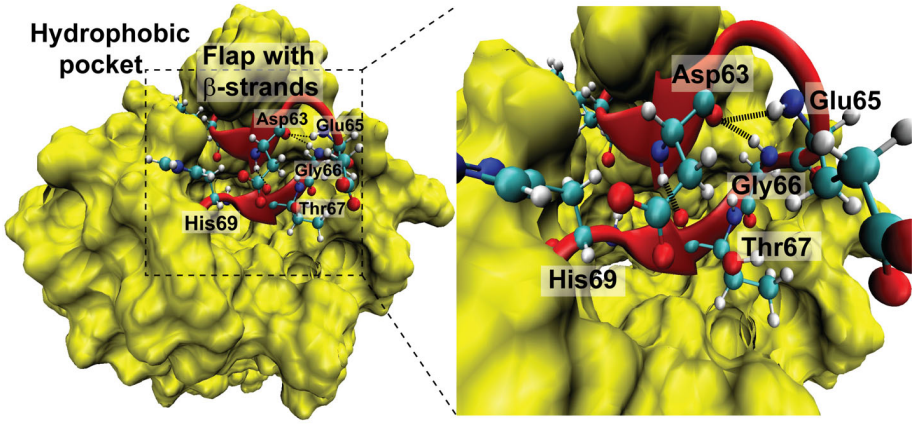

FIGURE 6 Close-up view of the β-flap covering the binding pocket. Residues Asp63, Glu65, Gly66, Thr67, and His69 that form hydrogen bonds are shown by dashed lines. The figure was prepared using VMD

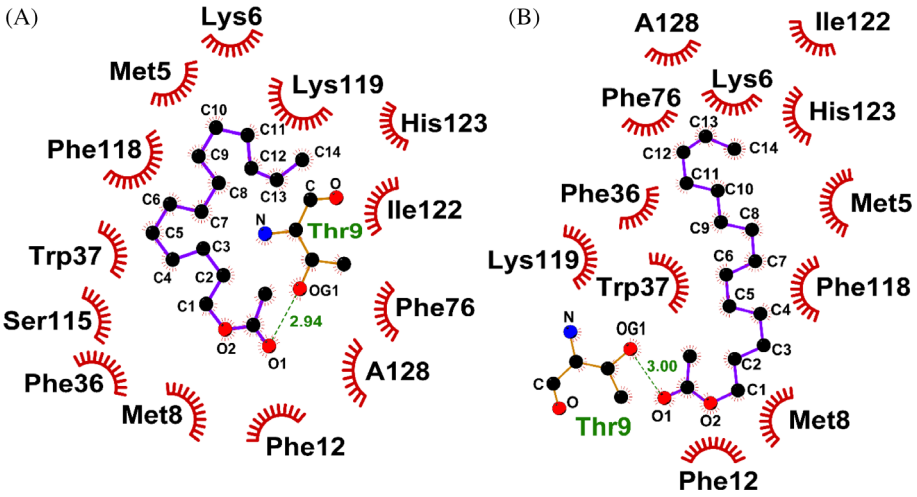

FIGURE 7 The view of interactions of amino acid sidechains in the binding pocket of OfurPBP2 with pheromone isomers. (A) The amino acids interacting with E-12-tetradecenyl acetate pheromone (B) The amino acids interacting with Z-12-tetradecenyl acetate pheromone. The hydrogen bond between the Thr9 sidechain and the acetate group of the pheromone is shown in dotted line. The figure was prepared using Ligplot

into a buried pocket. The lip of this pocket is elliptical with dimensions of 12 Å by 6 Å and is composed of mostly hydrophobic residues from L3 (Leu62, Gly66, and Leu68), α6 (Met110, Ala111, and Ile114), α3 (Leu53 and Ser56), and α5 (Val94). The other end of the pocket lies in the interface of L2, α1, and α2 helices. The pocket is lined with the following residues: Met5, Lys6, Met8, Thr9, Phe12, and Ile13 of α1, Glu 32, Val33, Phe36, and Trp37 of α2, Ala 48, Ile52, Ser56 of α3, Leu61, Leu62, Thr67, and Leu68 of L3, Asn72, Thr73, Phe76, and Ala77 of α4, Leu90, and Val94 of α5, and Ala111, Leu112, Ile114, Ser115, Phe118, and Lys119 of α6, and Ala128 from L6.

There are two openings to the hydrophobic pocket of OfurPBP2: (i) the flexible flap (61–69), Arg70, and the His88 situated at one end of the cavity (ii) the C-terminal amphipathic helix (His131-Lys143) at the other end (Figure S6B). The C-terminal helix is 18.7 Å long; it is composed of six charged residues that include five negatively charged residues (Asp130, Glu132, Glu136, Glu137, and Glu141) and one positively charged residue at pH 6.5 (Lys143). The charged residues lie on the same face of the helix, giving it an amphipathic character (Figure S6B).

2.6 | Molecular docking

The molecular docking studies of OfurPBP2 with each pheromone isomer suggests that, in the lowest energy docking pose, both tpheromones assume a U-shape to be accommodated in the pocket. The E-isomer interacts with Met5, Lys6, Met8, Thr9, Phe12, Phe36, Trp37, Phe76, Ser115, Phe118, Lys119, Ile122, His123, and Ala128 while the Z-isomer interacts with Met5, Lys6, Met8, Thr9, Phe12, Phe36, Trp37, Phe76, Phe118, Lys119, Ile122, and Ala128. These poses predict that the sidechain of Thr9 forms a hydrogen bond with the acetate group of the ligand with an O-O the distance of 2.94 Å (*E*) and 3.00 Å (*Z*) (Figure 7).

3 | DISCUSSION

The 3D structure of OfurPBP2 (Figure 4) reported here is the first high-resolution PBP structure in an *Ostrinia* species. The structure of OfurPBP2 at pH 6.5 has distinct structural features compared to other well-studied

lepidopteran PBPs.[16,23,26] The core of the protein has a similar architecture to that of ApolPBP1,[16] BmorPBP,[26] and AtraPBP1[23] with an rmsd of 4.29, 1.95, and 1.86, respectively. However, the C-terminus of OfurPBP2 forms an amphipathic helix in contrast to ApolPBP1,[16] BmorPBP,[26] and AtraPBP1.[23] Surprisingly, *Bombyx mori* general odorant-binding protein 2 (BmorGOBP2)[28] has a long amphipathic C-terminal α-helix similar to OfurPBP2, although these two proteins have only 29% sequence identity.

In many lepidopteran PBPs, including ApolPBP1, BmorPBP, and Atra PBP1, His70 and His95 are strictly conserved and act as a pH-dependent molecular switch that in part regulates the characteristic conformational change associated with ligand binding and release. Although OfurPBP2 has about 50% sequence identity with ApolPBP1,[16] BmorPBP,[26] and AtraPBP1[23] including six strictly conserved cysteine residues, there are major differences in the two biological gates (Figure 1). In ApolPBP1, BmorPBP, and AtraPBP1, the two biological gates are: (i) histidine gate composed of His70 and His95 (ii) C-terminal gate encompassing residues Pro129-Val142.[20] These two gates have been implicated in ligand-binding and release mechanisms.[20,21] However, the His70 in the histidine gate is substituted with an Arg in OfurPBP2. In fact, there are several lepidopteran odorant binding proteins (OBPs) that have His70 substituted with either an arginine (*Helicoverpa armigera* OBP15[29] and *Papilio xuthus* GOBP[30]) or with a lysine (*Maruca vitrata* PBP2[31] and *Conogethes punctiferalis* PBP1).[32] Furthermore, in OfurPBP2 there is a His88 residue in α5 helix that is not present in the other PBPs.[16,23,26] In OfurPBP2 NMR structure, Arg70, His88, and His95 are located close to the base of the flap. The distance between Arg70 and His88 is about 4.3 Å. At pH 6.5, Arg70 is positively charged and form a cation–π interaction (His-Arg+, Figure 8)[33–35] with His88 in the open or PBP^B conformation. The Arg70 is closer to His88 (4.3 Å) than His95 (9.3 Å; Figure 8). The distance between His70 and His95 in the histidine gate of ApolPBP1 is 8.1 Å,[16] and 11.4 Å in AtraPBP1,[23] which suggests that His95 in OfurPBP2 may also participate in the cation–π interaction with Arg70. Based on our pH 6.5 structure, it is clear that Arg70-His88 gate likely performs the same function as the His70-His95 gate in ApolPBP1, BmorPBP, and AtraPBP1 at near-physiological pH in PBP^B conformation.

The core of the 3D structure of OfurPBP2 encapsulates a large horseshoe-shaped hydrophobic pocket (Figure 5) formed by the six helices (α1–α6) along with the loops L3 (the flap) and L6. This pocket is lined with 30 amino acid residues from α1 to α6, and L6 that are mostly hydrophobic. This pocket is suitable to bind, protect, and transport the hydrophobic pheromones to the olfactory receptor site. The hydrophobic pheromones of OfurPBP2 are geometric isomers consisting of an unsaturated C-14 aliphatic chain with an acetate (-$OCOCH_3$) headgroup.[12] In contrast, the pheromones of *Bombyx mori*,[26] *Amyelois transitella*,[23] and *Antheraea polyphemus*[16,36] are not isomers and contain an alcohol (Bmor), or aldehyde (Atra), or acetate (Apol) as a headgroup with an unsaturated C-16 chain. While most of the hydrophobic residues that stabilize the pheromone in the pocket are conserved in moth PBPs, the residues that form hydrogen bonds with the head group vary among species: Ser56 in BmorPBP,[26] Asn53 in ApolPBP1,[16] and Arg107 in AtraPBP1.[23] Molecular docking studies revealed that the hydroxyl group of Thr9 in OfurPBP2 forms a hydrogen bond with the acetate head group of both *E*- and *Z*- pheromones (Figure 7). OfurPBP2 with a 14-carbon chain (C-14) pheromone has Met8 and Thr9 in the binding pocket in place of Leu8 and Ser9, which are present in PBPs that bind to a 16-carbon (C-16) pheromone. This observation is consistent with a previous suggestion that Met8 and Thr9 with bulky sidechains replace the less bulky Leu8 and Ser9 to reduce the volume of the pocket, making it favorable for shorter-chain pheromones.[16] Indeed, at pH 6.5 the OfurPBP2 had nanomolar binding affinity towards both E12-14: OAc and Z12–14: OAc pheromones. OfurPBP2 has slightly higher affinity to Z-isomer of the pheromone (33.5 nM) than the E-isomer (47.3 nM).

Lepidopteran PBPs bind and release the pheromone through a pH-dependent conformational switch.[15,16,18–23,26,36–57] These PBPs are in the PBP^B conformation at neutral pH when bound to the hydrophobic ligand but switches to a well-defined PBP^A conformation at low pH when the ligand is released.[16,19–21,36,37,39,40,42,43] We have previously reported that OfurPBP2[14,17] undergoes reversible pH-dependent conformational change akin to ApolPBP1, BmorPBP, AtraPBP1, and LdisPBP2. However, unlike these other PBPs,[16,19–21,36,37,39,40,42,43] OfurPBP2 does

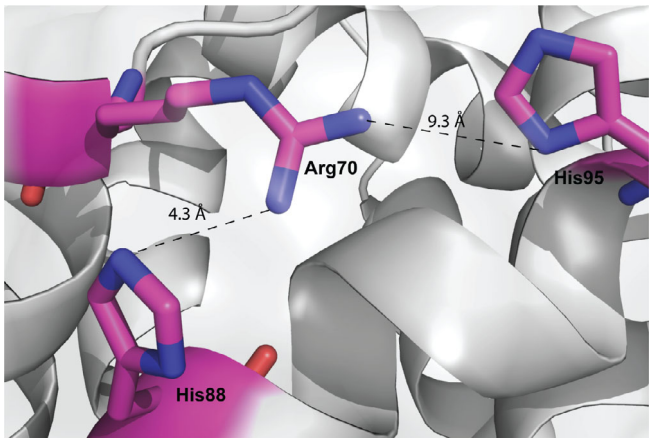

FIGURE 8 Stick representations of the sidechains of Arg70, His88, and His95, showing the formation of cation–pi interactions

not switch to a well-defined PBP^{A} conformation at pH 4.5. Instead, partial unfolding or a molten globule-like state has been reported during pH titration studies with NMR, which is also consistent with the far-UV CD data of OfurPBP2 at pH 6.5 and 4.5 as reported previously.[14] Although, there is a decrease in the magnitude of negative ellipticity at pH 4.5, the protein maintains 75% of helical structure compared to that at pH 6.5 based on deconvolution of CD spectra using DICROWEB.[58] Intramolecular disulfide bonds are known to provide structural stability to proteins even in denatured state.[59,60] The three intramolecular covalent bonds involving Cys19–Cys54, Cys50–Cys108, and Cys-97–Cys-117 that hold α1, α3, α5 and α6 helices of OfurPBP2 in place play a critical role in maintaining the overall architecture of the protein in the molten globule state at acidic pH. Indeed, the melting point of OfurPBP2 at pH 4.5 is very close to the melting point at pH 6.5 (87 and 90°C, respectively) suggesting that the overall architecture of the protein is maintained in the molten globule state at acidic pH. Thus, the unfolding process of the protein at pH 4.5 is expected to be similar to that at pH 6.5.

Indeed, *Ostrinia nubilalis* PBP3(OnubPBP3) behaves in a similar manner.[24] It seems likely that at acidic pH, the protonated His88 would disrupt the cation–π interactions with Arg70. In addition, the repulsion between the positively charged His88 (α5) and His95 (α5) would disrupt the helix, causing it to unwind and unfold partially at pH 4.5. Additionally, the C-terminal gate (Pro129–Lys143) of OfurPBP2 has seven charged residues at pH 4.5 (Asp130, His131, Glu132, Glu136, Glu137, Glu141, and Lys143) as opposed to the three charged residues (Asp132, Glu137, and Glu141) for ApolPBP1, BmorPBP, and AtraPBP1. Thus, the C-terminus of OfurPBP2 is less hydrophobic than the other PBPs. This could explain the inability of OfurPBP2 to switch conformation at low pH. Indeed, partial unfolding to a molten globule-like state may be the key to ligand release in OfurPBP2.

In order to further verify the structural stability of OfurPBP2 at two different pH (6.5 and 4.5), thermal unfolding of OfurPBP2 was carried out using circular dichroism (CD) to determine the thermodynamic parameters. In the far-UV CD, we observed a gradual decrease in the ellipticities of the characteristic minima at 208 and 222 nm of OfurPBP2 with increasing temperature (Figure S4). The two-state nature of the unfolding transition is evident due to the presence of an isodichroic point at 203 nm in both heating and cooling curves at pH 6.5 and 4.5 (Figure S4). Moreover, the similarity in the heating and cooling curves (Figure S4) at both pH values suggest the reversibility of the unfolding process. The slope of the unfolding curve qualitatively determines the cooperativity in the unfolding transition. A highly cooperative unfolding transition indicates the initial existence of the protein in a compact, well-folded structure. The sigmoidal curve at pH 4.5 has a smaller slope (0.6) compared to pH 6.5 (0.9) indicating a less cooperative unfolding of the protein at low pH (Figure 3).[61] This suggests that at pH 4.5, the protein exists in a flexible form. The thermodynamic parameters of unfolding at pH 6.5 and 4.5 were compared to get detailed insight into protein stability. Although the T_m at pH 6.5 was slightly higher than that of at pH 4.5, other thermodynamic properties such as ΔG, ΔH, and ΔS of unfolding were significantly different. The free energy change of unfolding ($\Delta G_{unfolding}$) and enthalpy change ($\Delta H_{unfolding}$) were: 47.1 ± 1.9 and 262.8 ± 10.5 kJ/mol at pH 6.5; 32.3 ± 0.8 and 186.4 ± 4.8 kJ/mol at pH 4.5, respectively. These values indicate a non-spontaneous unfolding. The reduction in $\Delta G_{unfolding}$ and $\Delta H_{unfolding}$ at pH 4.5 is a clear indication of the decrease in structural stability or disruption of tertiary structure at pH 4.5. Furthermore, at pH 4.5, the entropy of unfolding ($\Delta S_{unfolding}$) at equilibrium ($\Delta G = 0$) is 208 J/mol K less as compared to that at pH 6.5, which demonstrates unfolding of the protein from a less compact state. In conclusion, the reduction in $\Delta S_{unfolding}$, $\Delta H_{unfolding}$, $\Delta G_{unfolding}$, and cooperativity of unfolding at pH 4.5 reveals that the protein exists in a more flexible form or in a molten globule state. At acidic pH, electrostatic repulsions could be a driving force for the collapse of the native tertiary structure. The thermodynamic data are consistent with what was observed previously in our pH-titration studies with NMR.[14] In addition, the lack of affinity of OfurPBP2 at pH 4.5 to the pheromones strongly supports the loss of tertiary structure (Figure S2). Taken together, it appears that the ligand release in OfurPBP2 occurs through partial unfolding of the protein at acidic pH. This proposed mechanism of ligand release in OfurPBP2 is different from the ligand release mechanism reported for several well-studied Lepidopteran PBPs. In these PBPs, charge repulsion between the protonated histidines (His70 and His95) at acidic pH opens the His gate while the newly formed C-terminal helix outcompetes the ligand for the hydrophobic pocket releasing it through the opened His gate.[16,19–21,36,37,39,40,42,43] Thus, these proteins unlike OfurPBP2 form a well-defined ligand-releasing conformation at low pH.

4 | METHODS

4.1 | Sample preparation

Uniformly isotopically labeled (^{15}N and $^{15}N/^{13}C$), recombinant OfurPBP2 was expressed in *E.coli* and purified by ion exchange and size exclusion chromatography as described previously.[14,17] NMR samples used for the structure determination contained 0.4 mM protein solution in 90% H_2O/10% D_2O in 50 mM

phosphate buffer at pH 6.5 containing 1 mM EDTA and 0.1% NaN_3.

4.2 | Thermal unfolding by circular dichroism

Thermally induced equilibrium unfolding was monitored by measurement of the change in mean residual ellipticity at 222 nm using a Jasco 815 Circular Dichroism (CD) Spectropolarimeter in Dr. Smita Mohanty's laboratory, Chemistry Department at Oklahoma State University or with a Jasco 715 CD Spectropolarimeter in the core facility of Department of Biochemistry & Molecular Biology at University of Oklahoma Health Sciences Center. For thermal scans, 30 μM protein samples in a 0.05 cm quartz cuvette at pH 6.5 and 4.5 were heated from room temperature to 110°C. The temperature was ramped at the rate of 2°C/min controlled by a Jasco programmable Peltier element. A scan rate of 1°C/min was taken. Far-UV CD spectra were recorded at 2°C or 5°C increments and the dichroic activity at 222 nm was continuously monitored every 2°C with a 4 s averaging time. All the spectra were corrected for the buffer used. For the melting temperature (T_m), the fraction of the protein unfolded with increasing temperature was fitted with a Boltzmann function for perfect sigmoidal line shapes. Here the midpoint of the unfolding transition reflects the T_m. However, other thermodynamic properties ($\Delta H_{unfolding}$, $\Delta G_{unfolding}$, etc.) were calculated by fitting the variation of ellipticity at 222 nM with temperature into the Gibbs–Helmholtz equation that illustrates protein folding as a function of temperature.[62] The best fit values to the raw data were extracted using the fitting procedure in Origin.[63]

4.3 | Delipidation

OfurPBP2 was delipidated using a protocol modified from prior work.[21,24] Briefly, OfurPBP2 in 50 mM sodium citrate buffer (buffer A) at pH 4.5 was loaded to a column packed with Lipidex-1000 and equilibrated in buffer A. The column loaded with the protein was incubated at 37°C for 30 min. The protein was eluted from the column with buffer A. The eluted protein was concentrated, and buffer exchanged to 20 mM sodium phosphate buffer at pH 6.5 for fluorescence studies.

4.4 | Fluorescence spectroscopy

The fluorescence binding assay was performed on a PerkinElmer LS 55 Fluorescence Spectrophotometer at room temperature with a 1 cm light-path quartz cuvette. The emission slit width of 7.0 nm and excitation slit width of 4.5 nm was used. Each spectrum was average with 5 scans at a speed of 500 nm/min. The fluorescence measurements were carried out in 20 mm phosphate buffer at pH 6.5 or 4.5.

The binding of extrinsic fluorescent probe (NPN) to delipidated OfurPBP2 at pH 6.5 was reported previously by monitoring the increase in the NPN fluorescence at 420 nm.[63] The competitive displacement of NPN from OfurPBP2:NPN complex with *E*-12 or *Z*-12-tetradecenyl acetate pheromone was performed to determine the affinity of each pheromone to OfurPBP2 at pH 6.5. All experiments were repeated at least three times to confirm reproducibility. Briefly, 2 μM delipidated OfurPBP2 was equilibrated overnight with 2 μM NPN at 4°C, which were then titrated individually with 1.0 mM stock of *E*-12 or *Z*-12 pheromone dissolved in methanol. The pheromones are hydrophobic small organic molecules that are soluble in organic solvents. Methanol was found to be suitable as it is miscible in water/buffer with a minimum effect on the protein up to 5% v/v.[21] All measurements for the binding assay contain ~0.3% of methanol in the total volume of the sample (v/v). Decrease in NPN fluorescence was monitored with addition of increasing concentration of pheromone from a 1 mM stock. NPN fluorescence was recorded with an excitation wavelength of 337 nm and the emission of 370–600 nm. After each addition, the complex was incubated for 10 min before recording the spectrum. Appropriate controls were recorded to correct each spectrum. The assay was performed in triplicate sets. The decrease in the fluorescence intensity of NPN at the λ_{max} (420 nm) was calculated as $(F_C - F_{min})/(F_o - F_{min})$, where F_o is the initial fluorescence intensity of NPN-OfurPBP2 complex; F_C is the corrected fluorescence intensity at a ligand concentration (C), and F_{min} is the fluorescence intensity at the saturating concentration of the competitor. The plot of $(F_C - F_{min})/(F_o - F_{min})$ against (C) (Figure 2) was fitted using the nonlinear fitting module of Origin 2019 to obtain IC_{50} using the equation provided below.[14,21]

$$y = 1 - x/(k + x)$$

where k is the IC_{50}, x is the pheromone concentration, and y is the fluorescence intensity at the specific ligand concentration. The ligand concentrations at which the NPN fluorescence was quenched to half of its maximal intensity provided the IC_{50} values. The dissociation constant (K_d) was calculated using the equation: $K_d = [IC_{50}]/(1 + [NPN]/K_{NPN})$, where [NPN] is the free concentration of NPN and K_{NPN} is the dissociation constant for

protein–NPN complex.[64] The fluorescence binding assay at pH 4.5 was carried out in a similar manner.

4.5 | NMR spectroscopy and resonance assignment

All NMR data were acquired at 35°C on a Bruker Avance II 800 MHz spectrometer equipped with a triple resonance H/C/N cryoprobe TCI with pulse field gradients at the National High Magnetic Field Laboratory (NHMFL) at Tallahassee, FL. The following experiments were performed for sequential assignments[17] and structure analysis: 2D {^{1}H, ^{15}N} HSQC, 2D {^{1}H, ^{13}C} HSQC, 3D HNCA, 3D HN(CO)CA, 3D HNCO, 3D HN(CA)CO, 3D HNCACB, 3D CACB(CO)NH, 3D CC(CO)NH, 3D H(CCCO)NH, 3D HCCH-TOCSY, 3D ^{15}N-edited HSQC TOCSY, 3D ^{15}N-edited HSQC- NOESY (T_m = 85 ms) and 3D ^{13}C-edited HSQC-NOESY (T_m = 120 ms). In the ^{13}C-edited NOESY, the ^{13}C carrier frequency was set to 43 ppm for the aliphatic and 125 ppm for the aromatic region. The NMR data were processed using NMRPipe[65] and analyzed with NMRFAM SPARKY.[66]

4.6 | NOE assignments and structure calculation

NOE peaks were manually peak-picked and integrated interactively. The 2,557 NOE cross-peaks were assigned using NMRFAM-SPARKY. Structure calculation was carried with CYANA 3.98.13.[67] The assignments were confirmed or corrected with CYANA, using the standard protocol of seven cycles of iterative NOE assignment and structure calculation.[67] A total of 260 upper-limit constraints based on backbones dihedral angle (φ and ψ) were determined from TALOS+,[68] and standard upper and lower distant constraints for three disulfide bonds were used. During the iterative NOE assignment, 446 NOEs were corrected, 80 were removed, and 375 were added, resulting in a total of 2,557 assigned NOE cross-peaks. The experimentally derived upper distance restraints were derived from the NOE intensities using two calibration functions of d^{-6} for the backbone and d^{-4} for the sidechain resonances of the assigned peaks. There are 402 long-range NOEs. The calculation was started with 100 initial conformers, and the 20 conformers with the lowest residual target were used for energy minimization with YASARA[69] by using the YASARA force field.[70] The 20 structures with the lowest potential energy and best Ramachandran plot score were assessed by Molprobity[71] and PROCHECK.[72] Complete statistics are given in Table 1.

4.7 | Molecular docking studies

Molecular docking studies were performed to predict the potential binding mode and to estimate the free energy of binding of the OfurPBP2 and the pheromones molecule. Docking was performed using AutoDock.[73] AutoDock Tools 1.5.6 was used to create the PDBQT format. Polar hydrogens were added using the AutoDock Tools interface. All torsion was released except around the double bond. The default AutoDock force field was employed.[74] The protein pocket was covered by a grid box with a spacing of 0.375 Å. For the genetic algorithm, default parameters were used. Each ligand was subjected to 200 Lamarckian genetic algorithm runs, with 25×10^6 evaluations in each and the rest of the parameters were default. The root means square deviation (rmsd) tolerance of the resulting docked structures was ≤2 Å. AutoDock performs cluster analysis based on all-atom root mean square deviation (rmsd). The resulting families of docked conformations were ranked according to increasing energy. The pose with the most populated cluster was selected for the analysis.[75]

4.8 | Statistics and visualization

Visualization, root-mean-square distance, hydrogen bond, and helix packing angle calculations were performed with the programs PYMOL, Chimera, MOL MOL, and VMD. Ramachandran plot statistics were calculated by PROCHECK.

4.9 | PDB and BRMB accession codes

The atomic coordinates of OfurPBP2 have been deposited to the Protein Data Bank† (accession code 7UO6) and BMRB ID 30762. The assigned chemical shifts have been deposited in the BioMagResBank‡ (accession code 57004).

AUTHOR CONTRIBUTIONS

Salik Dahal: Formal analysis (equal); investigation (equal); validation (equal); visualization (equal); writing – original draft (equal). **Jacob Lewellen:** Formal analysis (equal); investigation (equal); validation (equal); visualization (equal); writing – original draft (equal). **Shine Ayyappan:** Formal analysis (equal); validation (supporting); visualization (supporting); investigation (supporting), writing – original draft (equal); writing – review and editing (equal). **Bharat Chaudhary:** Formal analysis (supporting); investigation (supporting); visualization (equal); writing – review and editing (equal). **Viswanath**

Nukala: Investigation (supporting). **Smita Mohanty:** Conceptualization (lead); formal analysis (supporting); investigation (lead); project administration (lead); resources (lead); supervision (lead); validation (supporting); visualization (supporting); writing – original draft (equal); writing – review and editing (lead).

ACKNOWLEDGMENTS

This research was financially supported by National Science Foundation Award CHE-1807722 and DBI-1726397 to Smita Mohanty. Most of the NMR data were collected at the National High Magnetic Field Laboratory, which is supported by the National Science Foundation Cooperative Agreement No. DMR-1644779 and the State of Florida. We thank Dr. David Zoetewey of Georgia College and State University for useful suggestions and discussions during the structure calculations process, Drs. Karla Rodgers and Jennifer Byrum of University of Oklahoma Health Sciences Center for providing access to CD instrument, Dr. Thomas Webb of Auburn University for critical reading of the manuscript, and Ms. Pratikshya Paudel for help with protein refolding.

CONFLICT OF INTEREST

The authors declare that they have no conflict of interest with the contents of this article.

ORCID

Smita Mohanty https://orcid.org/0000-0002-1680-6338

REFERENCES

1. Greenfield MD. Moth sex pheromones: An evolutionary perspective. Fla Entomol. 1981;64:4–17.
2. Butenandt A. Bombykol, the sex-attractive substance of the silk worm, Bombyx mori. Annual Lecture 1962 before the Society of Endocrinology, Proceedings of the Society of Endocrinology 1963; p. 9.
3. Vogt RG. The molecular basis of pheromone reception: Its influence on behavior. Pheromone Biochemistry. Cambridge, MA: Academic Press, 1987; p. 385–431.
4. Hutchison WD, Burkness EC, Mitchell PD, et al. Areawide suppression of European corn borer with Bt maize reaps savings to non-Bt maize growers. Science. 2010;330:222–225.
5. Zalucki MP, Shabbir A, Silva R, Adamson D, Shu-Sheng L, Furlong MJ. Estimating the economic cost of one of the World's major insect pests, Plutella xylostella (Lepidoptera: Plutellidae): Just how long is a piece of string? J Econ Entomol. 2012;105:1115–1129.
6. Zhang T, He K, Wang Z. Transcriptome comparison analysis of *Ostrinia furnacalis* in four developmental stages. Sci Rep. 2016; 6:35008.
7. Smita M, Joshua RR, Rabi KP. Chemical communication: A visit with insects. Curr Chem Biol. 2008;2:83–96.
8. Allen JE, Wanner KW. Asian corn borer pheromone binding protein 3, a candidate for evolving specificity to the 12-tetradecenyl acetate sex pheromone. Insect Biochem Mol Biol. 2011;41:141–149.
9. Willett CS, Harrison RG. Pheromone binding proteins in the European and Asian corn borers: No protein change associated with pheromone differences. Insect Biochem Mol Biol. 1999;29: 277–284.
10. Roelofs WL, Liu W, Hao G, Jiao H, Rooney AP, Linn CE. Evolution of moth sex pheromones via ancestral genes. Proc Natl Acad Sci. 2002;99:13621–13626.
11. Yeh SF, Lee KC, Chang KT, Yen FC, Hwang JS. Sex pheromone components from Asian corn borer,*Ostrinia furnacalis* (Hubner) (Lepidoptera: Pyralidae) in Taiwan. J Chem Ecol. 1989;15:497–505.
12. Klun JA, Bierl-Leonhardt BA, Schwarz M, et al. Sex pheromone of the Asian corn borer moth. Life Sci. 1980;27:1603–1606.
13. Leary GP, Allen JE, Bunger PL, et al. Single mutation to a sex pheromone receptor provides adaptive specificity between closely related moth species. Proc Natl Acad Sci U S A. 2012; 109:14081–14086.
14. Mazumder S, Dahal SR, Chaudhary BP, Mohanty S. Structure and function studies of Asian corn borer *Ostrinia furnacalis* pheromone binding protein 2. Sci Rep. 2018;8:17105.
15. Terrado M, Okon M, McIntosh LP, Plettner E. Ligand- and pH-induced structural transition of Gypsy Moth Lymantria dispar pheromone-binding protein 1 (LdisPBP1). Biochemistry. 2020; 59:3411–3426.
16. Mohanty S, Zubkov S, Gronenborn AM. The solution NMR structure of Antheraea polyphemus PBP provides new insight into pheromone recognition by pheromone-binding proteins. J Mol Biol. 2004;337:443–451.
17. Dahal SR, Lewellen JL, Chaudhary BP, Mohanty S. (1)H, (13) C, and (15)N resonance assignment and secondary structure of the pheromone-binding protein2 from the agricultural pest *Ostrinia furnacalis* (OfurPBP2). Biomol NMR Assign. 2020;14: 115–118.
18. Lee D, Damberger FF, Peng G, et al. NMR structure of the unliganded Bombyx mori pheromone-binding protein at physiological pH. FEBS Lett. 2002;531:314–318.
19. Xu X, Xu W, Rayo J, Ishida Y, Leal WS, Ames JB. NMR structure of navel orangeworm moth pheromone-binding protein (AtraPBP1): Implications for pH-sensitive pheromone detection. Biochemistry. 2010;49:1469–1476.
20. Katre UV, Mazumder S, Mohanty S. Structural insights into the ligand binding and releasing mechanism of Antheraea polyphemus pheromone-binding protein 1: Role of the C-terminal tail. Biochemistry. 2013;52:1037–1044.
21. Katre UV, Mazumder S, Prusti RK, Mohanty S. Ligand binding turns moth pheromone-binding protein into a pH sensor: Effect on the Antheraea polyphemus PBP1 conformation. J Biol Chem. 2009;284:32167–32177.
22. Lautenschlager C, Leal WS, Clardy J. Bombyx mori pheromone-binding protein binding nonpheromone ligands: Implications for pheromone recognition. Structure. 2007;15: 1148–1154.
23. di Luccio E, Ishida Y, Leal WS, Wilson DK. Crystallographic observation of pH-induced conformational changes in the Amyelois transitella pheromone-binding protein AtraPBP1. PLoS One. 2013;8:e53840.

24. Al-Danoon O, Mazumder S, Chaudhary BP, et al. Structural and functional characterization of European corn borer, Ostrinia nubilalis, pheromone binding protein 3. J Agric Food Chem. 2021;69:14013–14023.
25. Sharma D, Rajarathnam K. 13C NMR chemical shifts can predict disulfide bond formation. J Biomol NMR. 2000;18:165–171.
26. Sandler BH, Nikonova L, Leal WS, Clardy J. Sexual attraction in the silkworm moth: Structure of the pheromone-binding-protein-bombykol complex. Chem Biol. 2000;7:143–151.
27. Rötzschke O, Lau JM, Hofstätter M, Falk K, Strominger JL. A pH-sensitive histidine residue as control element for ligand release from HLA-DR molecules. Proc Natl Acad Sci. 2002;99:16946–16950.
28. Zhou JJ, Robertson G, He X, et al. Characterisation of Bombyx mori odorant-binding proteins reveals that a general odorant-binding protein discriminates between sex pheromone components. J Mol Biol. 2009;389:529–545.
29. Liu Y, Gu S, Zhang Y, Guo Y, Wang G. Candidate olfaction genes identified within the Helicoverpa armigera antennal transcriptome. PLoS One. 2012;7:e48260.
30. Ozaki K, Utoguchi A, Yamada A, Yoshikawa H. Identification and genomic structure of chemosensory proteins (CSP) and odorant binding proteins (OBP) genes expressed in foreleg tarsi of the swallowtail butterfly Papilio xuthus. Insect Biochem Mol Biol. 2008;38:969–976.
31. Malini P, Ramasamy S, Schafleitner R, Muthukalingan K. Pheromone-binding proteins based phylogenetics and phylogeography of Maruca spp. from Asia, Africa, Oceania, and South America. Ecol Evol. 2019;9:9239–9272.
32. Xiao-Jian Jia H-XW, Yan Z-G, Zhang M-Z, et al. cDNA cloning, expression profiling and binding affinity assay of the pheromone binding protein Cpun-PBP1 in the yellow peach moth, Conogethes punctiferalis (Lepidoptera: Crambidae). Acta Entomol. 2015;58:1167–1176.
33. Liao SM, Du QS, Meng JZ, Pang ZW, Huang RB. The multiple roles of histidine in protein interactions. Chem Cent J. 2013;7:44.
34. Kumar K, Woo SM, Siu T, Cortopassi WA, Duarte F, Paton RS. Cation–π interactions in protein–ligand binding: Theory and data-mining reveal different roles for lysine and arginine. Chem Sci. 2018;9:2655–2665.
35. Hou Q, Bourgeas R, Pucci F, Rooman M. Computational analysis of the amino acid interactions that promote or decrease protein solubility. Sci Rep. 2018;8:14661.
36. Zubkov S, Gronenborn AM, Byeon IJ, Mohanty S. Structural consequences of the pH-induced conformational switch in A. polyphemus pheromone-binding protein: Mechanisms of ligand release. J Mol Biol. 2005;354:1081–1090.
37. Damberger FF, Ishida Y, Leal WS, Wuthrich K. Structural basis of ligand binding and release in insect pheromone-binding proteins: NMR structure of Antheraea polyphemus PBP1 at pH 4.5. J Mol Biol. 2007;373:811–819.
38. Mazumder S, Chaudhary BP, Dahal SR, Al-Danoon O, Mohanty S. Pheromone perception: Mechanism of the reversible coil–helix transition in Antheraea polyphemus pheromone-binding protein 1. Biochemistry. 2019;58:4530–4542.
39. Wojtasek H, Leal WS. Conformational change in the pheromone-binding protein from Bombyx mori induced by pH and by interaction with membranes. J Biol Chem. 1999;274:30950–30956.
40. Damberger F, Nikonova L, Horst R, Peng G, Leal WS, Wuthrich K. NMR characterization of a pH-dependent equilibrium between two folded solution conformations of the pheromone-binding protein from Bombyx mori. Protein Sci. 2000;9:1038–1041.
41. Leal WS. Duality monomer-dimer of the pheromone-binding protein from Bombyx mori. Biochem Biophys Res Commun. 2000;268:521–529.
42. Horst R, Damberger F, Luginbuhl P, et al. NMR structure reveals intramolecular regulation mechanism for pheromone binding and release. Proc Natl Acad Sci U S A. 2001;98:14374–14379.
43. Lautenschlager C, Leal WS, Clardy J. Coil-to-helix transition and ligand release of Bombyx mori pheromone-binding protein. Biochem Biophys Res Commun. 2005;335:1044–1050.
44. Leal WS, Chen AM, Ishida Y, et al. Kinetics and molecular properties of pheromone binding and release. Proc Natl Acad Sci U S A. 2005;102:5386–5391.
45. Gräter F, de Groot BL, Jiang H, Grubmüller H. Ligand-release pathways in the pheromone-binding protein of Bombyx mori. Structure. 2006;14:1567–1576.
46. Xu W, Leal WS. Molecular switches for pheromone release from a moth pheromone-binding protein. Biochem Biophys Res Commun. 2008;372:559–564.
47. Michel E, Damberger FF, Ishida Y, et al. Dynamic conformational equilibria in the physiological function of the Bombyx mori pheromone-binding protein. J Mol Biol. 2011;408:922–931.
48. Damberger FF, Michel E, Ishida Y, Leal WS, Wüthrich K. Pheromone discrimination by a pH-tuned polymorphism of the Bombyx mori pheromone-binding protein. Proc Natl Acad Sci U S A. 2013;110:18680–18685.
49. Xu X, Li Y, Rayo J, Ishida Y, Leal W, Ames JB. 1H, 15N, and 13C chemical shift assignments of the navel orange worm pheromone-binding protein-1 (Atra-PBP1). Biomol NMR Assign. 2008;2:105–106.
50. Xu W, Xu X, Leal WS, Ames JB. Extrusion of the C-terminal helix in navel orangeworm moth pheromone-binding protein (AtraPBP1) controls pheromone binding. Biochem Biophys Res Commun. 2011;404:335–338.
51. Ziegelberger G. The multiple role of the pheromone-binding protein in olfactory transduction. Ciba Found Symp. 1996;200:267–275. discussion 275-80.
52. Plettner E, Lazar J, Prestwich EG, Prestwich GD. Discrimination of pheromone enantiomers by two pheromone binding proteins from the Gypsy Moth Lymantria dispar. Biochemistry. 2000;39:8953–8962.
53. Kowcun A, Honson N, Plettner E. Olfaction in the gypsy moth, Lymantria dispar: Effect of pH, ionic strength, and reductants on pheromone transport by pheromone-binding proteins. J Biol Chem. 2001;276:44770–44776.
54. Honson N, Johnson MA, Oliver JE, Prestwich GD, Plettner E. Structure–activity studies with pheromone-binding proteins of the Gypsy Moth, Lymantria dispar. Chem Senses. 2003;28:479–489.
55. Gong Y, Pace TCS, Castillo C, Bohne C, O'Neill MA, Plettner E. Ligand-interaction kinetics of the pheromone-

binding protein from the Gypsy Moth, *L. dispar*: Insights into the mechanism of binding and release. Chem Biol. 2009;16: 162–172.
56. Gong Y, Tang H, Bohne C, Plettner E. Binding conformation and kinetics of two pheromone-binding proteins from the Gypsy Moth Lymantria dispar with biological and nonbiological ligands. Biochemistry. 2010;49:793–801.
57. Yu Y, Ma F, Cao Y, et al. Structural and functional difference of pheromone binding proteins in discriminating chemicals in the gypsy moth, Lymantria dispar. Int J Biol Sci. 2012;8: 979–991.
58. Miles AJ, Ramalli SG, Wallace BA. DichroWeb, a website for calculating protein secondary structure from circular dichroism spectroscopic data. Protein Sci. 2022;31:37–46.
59. Hartig GR, Tran TT, Smythe ML. Intramolecular disulphide bond arrangements in nonhomologous proteins. Protein Sci. 2005;14:474–482.
60. Wiedemann C, Kumar A, Lang A, Ohlenschlager O. Cysteines and disulfide bonds as structure-forming units: Insights from different domains of life and the potential for characterization by NMR. Front Chem. 2020;8:280.
61. Neira JL, Contreras LM, de los Paños OR, et al. Structural characterisation of the natively unfolded enterocin EJ97. Protein Eng Des Sel. 2010;23:507–518.
62. Greenfield NJ. Using circular dichroism collected as a function of temperature to determine the thermodynamics of protein unfolding and binding interactions. Nat Protoc. 2006;1:2527–2535.
63. Origin(Pro), Version 2019. Northampton, MA: OriginLab Corporation.
64. Campanacci V, Krieger J, Bette S, et al. Revisiting the specificity of Mamestra brassicae and Antheraea polyphemus pheromone-binding proteins with a fluorescence binding assay. J Biol Chem. 2001;276:20078–20084.
65. Delaglio F, Grzesiek S, Vuister GW, Zhu G, Pfeifer J, Bax A. NMRPipe: A multidimensional spectral processing system based on UNIX pipes. J Biomol NMR. 1995;6:277–293.
66. Lee W, Tonelli M, Markley JL. NMRFAM-SPARKY: Enhanced software for biomolecular NMR spectroscopy. Bioinformatics. 2015;31:1325–1327.
67. Güntert P. Automated NMR protein structure calculation. Prog Nucl Magn Reson Spectrosc. 2003;43:105–125.
68. Shen Y, Delaglio F, Cornilescu G, Bax A. TALOS+: A hybrid method for predicting protein backbone torsion angles from NMR chemical shifts. J Biomol NMR. 2009;44:213–223.
69. Krieger E, Joo K, Lee J, et al. Improving physical realism, stereochemistry, and side-chain accuracy in homology modeling: Four approaches that performed well in CASP8. Proteins. 2009; 77(Suppl 9):114–122.
70. Essmann U, Perera L, Berkowitz ML, Darden T, Lee H, Pedersen LG. A smooth particle mesh Ewald method. J Chem Phys. 1995;103:8577–8593.
71. Williams CJ, Headd JJ, Moriarty NW, et al. MolProbity: More and better reference data for improved all-atom structure validation. Protein Sci. 2018;27:293–315.
72. Laskowski RA, Rullmannn JA, MacArthur MW, Kaptein R, Thornton JM. AQUA and PROCHECK-NMR: Programs for checking the quality of protein structures solved by NMR. J Biomol NMR. 1996;8:477–486.
73. Morris GM, Huey R, Lindstrom W, et al. AutoDock4 and AutoDockTools4: Automated docking with selective receptor flexibility. J Comput Chem. 2009;30:2785–2791.
74. Huey R, Morris GM, Olson AJ, Goodsell DS. A semiempirical free energy force field with charge-based desolvation. J Comput Chem. 2007;28:1145–1152.
75. Cosconati S, Forli S, Perryman AL, Harris R, Goodsell DS, Olson AJ. Virtual screening with AutoDock: Theory and practice. Expert Opin Drug Discov. 2010;5:597–607.

SUPPORTING INFORMATION

Additional supporting information can be found online in the Supporting Information section at the end of this article.

How to cite this article: Dahal SR, Lewellen JL, Ayyappan S, Chaudhary BP, Nukala V, Mohanty S. *Ostrinia furnacalis* PBP2 solution NMR structure: Insight into ligand binding and release mechanisms. Protein Science. 2022;31(10):e4438. https://doi.org/10.1002/pro.4438